POLITECNICO DI TORINO
Repository ISTITUZIONALE

Wall treatments for aeroacoustic measurements in closed wind tunnel test sections

(Article begins on next page)

26 December 2024

Wall treatments for aeroacoustic measurements in closed wind tunnel test sections

Hugo F. Mourão Bento[*,a], Colin P. VanDercreek[†,a], Francesco Avallone[‡,b], Daniele Ragni[§,a], Pieter Sijtsma[¶,a], and Mirjam Snellen[‖,a]

[a]*Delft University of Technology, Kluyverweg 1, Delft 2629 HS, The Netherlands*
[b]*Politecnico di Torino, Corso Duca degli Abruzzi 24, Torino 10129, Italy*

Aeroacoustic tests in closed wind tunnels are affected by reflections in the tunnel circuit and background noise. Reflections can be mitigated by lining the tunnel circuit. The present study investigates if lining exclusively the most accessible segment of a closed wind tunnel circuit, in particular the test section, is an approach which improves acoustic measurements. Literature shows that a wind tunnel lining material should have high acoustic absorption, low inertial resistivity and low surface roughness. Therefore, the test section of TU Delft's closed Low Turbulence Tunnel is lined with melamine foam wall liners. A total of 4 test section configurations were tested: baseline; test section with lining on the floor and ceiling; test section with lined side–panels; and test section lined at all surfaces (floor, ceiling and side–panels). An omnidirectional speaker is used for evaluating the wind tunnel's acoustic performance. A geometric modelling algorithm, based on the mirror-source method, is used to predict the effect of lining on primary reflections in the test section. In addition, reflections in the test section and in the tunnel circuit are characterized experimentally. The results show that the closed loop of the tunnel circuit is responsible for a long reverberation time in the test section. However, reflections inside the test section itself are the dominant source of acoustic interference at the microphone array location. The low fidelity geometric modelling algorithm is shown to be a valuable approach for an initial estimation of the acoustic benefit of lining, for both flow–off and –on conditions. Lining of the test section walls significantly reduces reflections from the reference source, as well as the aerodynamic background noise that reaches the array.

I. Introduction

Aeroacoustic measurements are frequently carried out in closed wind tunnel test sections, e.g. for studying wind turbine blade noise [1, 2], airframe noise [3] or propeller noise [4]. Since closed test sections do not experience jet deflection, or disturbances caused by the interaction between jet and collector, closed test sections provide a higher aerodynamic fidelity than open–jet test sections [5]. However, closed wind tunnels have a typically lower acoustic performance [6], e.g. due to reflections in the test section [7]. Possible solutions to reduce the detrimental effects of reflections are to line the facility's walls with sound absorbing materials [8], and to use post–processing methods which help identifying the main aerodynamic noise source of interest.

Acoustic beamforming techniques can quantify the noise from different sources in a (phased) microphone array measurement [9]. In this way, the detrimental effect of reflections of a direct source on the acoustic measurement can be reduced. Beamforming also improves the signal-to-noise ratio, e.g. with respect to aerodynamic background noise, in comparison with results obtained from single microphone measurements [10]. In closed wind tunnels, the tunnel walls' boundary layer aerodynamic noise is frequently a relevant source of noise [11]. The capability to separate a sound source of interest from spurious sources in the room depends on the resolution of each beamforming method. Conventional beamforming resolution is imposed by the Rayleigh limit [12], leading to a lower spatial resolution at low frequencies. Aeroacoustics research, conducted with the most advanced measurement and post–processing techniques, can therefore still benefit from the improvement of the acoustic behaviour of the testing facilities.

---

[*]PhD Candidate, TU Delft, Section Flow Physics and Technology (FPT)

[†]PhD, Section Aircraft Noise and Climate Effects (ANCE)

[‡]Assistant Professor, Politecnico di Torino, Department of Mechanical and Aerospace Engineering (DIMEAS)

[§]Associate Professor, TU Delft, Section Flow Physics and Technology (FPT)

[¶]Researcher, TU Delft, Section Aircraft Noise and Climate Effects (ANCE)

[‖]Full Professor, TU Delft, Section Aircraft Noise and Climate Effects (ANCE)

1

Aeroacoustic wind tunnel design solutions are extensively discussed in Ref. [13]. Lining of a wind tunnel circuit has a strong influence on the acoustic performance, and is often considered to be a justifiable investment. However, lining a closed wind tunnel with a porous material also affects the aerodynamic characteristics of the wind tunnel walls' boundary layer. An increase in the turbulence levels in the boundary layer can affect the scattering of spurious noise sources in the tunnel, e.g. from discontinuities [14]. The influence of porous materials on boundary layers is widely studied (e.g. by [15, 16]). The noise scattering from wind tunnel wall porous liners has been previously investigated. Literature [17] indicates that a good closed wind tunnel liner has a low surface roughness and inertial resistivity, and a high viscous resistivity, which leads to high acoustic absorption. Closed wind tunnel designs can benefit from research which assesses the improvement obtained from lining individual segments of the circuit, e.g. the diffraction or the test section.

The present study investigates the benefit of applying wall treatments to the test section of a closed wind tunnel. The study focuses on the trade-off between different lining configurations, with respect to a baseline (fully reflective) test case. Measurements of a known sound source (omnidirectional speaker) with each configuration, are used to assess the improvements achieved with each different lining. Measurements were taken with and without flow, in order to take into account the modifications in background noise. The experimental campaign was conducted in the Low Turbulence Tunnel (LTT), at TU Delft. The LTT is a closed wind tunnel intensively used for aerodynamic and aeroacoustic research, see e.g. [18–20].

The present document is structured as follows: Sec. II describes the facility, the measurement techniques, and post processing algorithms used. Section III presents and discusses the experimental results. Finally, Sec. IV highlights the main conclusions.

II. Methodology

A. Facility and models

The Low Turbulence Tunnel, at TU Delft, is a closed wind tunnel circuit, initially designed for aerodynamic testing. The circuit is powered by a six-bladed wind tunnel fan, which is connected with a 525 kW DC motor. The flow in the test section of 1.8 by 1.25 m can reach free-stream velocities, U_∞, up to $80 \, \text{m s}^{-1}$ with an average turbulence intensity, Tu, below 0.05 % [21]. The drive fan, the corner vanes, and the discontinuities on the walls of the test section and diffuser, respectively sections 1, 3a, 9, 10 and 11 (see Fig. 1a), are expected to be major sources of the background noise. Due to the closed form of the loop, reflections throughout the wind tunnel circuit contribute towards a long reverberation time, i.e. towards a prolongation of sound after each acoustic source has stopped emitting noise. Acoustic reflections in the test section are dictated by its elongated octagonal shape, which can be seen in the computer-aided design (CAD) diagram reported in Fig. 1b. Figures 1c and 1d show, respectively, the speaker installed in the baseline (fully reflective) test section and in the fully lined test section. The figures show that, for the aeroacoustic test section, the left side–panel is replaced by a Kevlar window, behind which the microphone array is placed.

1. Reference acoustic source

The acoustic source seen in Fig. 1 is a miniature QindW speaker model, developed by QSources [23]. The speaker has omnidirectionality at low frequencies, up to 2kHz [17]. The speaker is placed at the centre of the test section, being aligned with the streamwise centre of the microphone array. The aerodynamic shape of the speaker results in low aerodynamic self–noise.

For the flow-off tests, the speaker's input was based on an in–built white–noise signal, in the range 300 Hz to 6300 Hz. For the flow–on tests, the signal provided to the speaker was based on a sum of sine waves, with constant amplitudes, at the frequencies of interest. This solution allows for the increase of the speaker's noise signature at each frequency, f. Three distinct signals were provided to the speaker: a sum of sinusoids in the range $f_1 = 325 \, \text{Hz}$ to $f_{\text{end}} = 825 \, \text{Hz}$ (low–frequency, narrow band), a sum of sinusoids in the range $f_1 = 775 \, \text{Hz}$ to $f_{\text{end}} = 1275 \, \text{Hz}$ (mid–frequency, narrow band), and a sum of sinusoids in the range $f_1 = 325 \, \text{Hz}$ to $f_{\text{end}} = 2175 \, \text{Hz}$ (broadband). The signals, $v(t)$, were calculated from:
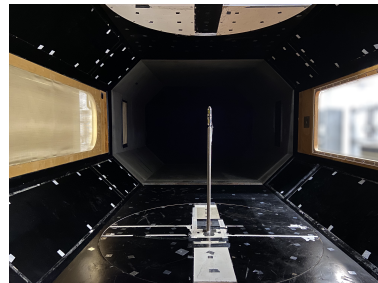
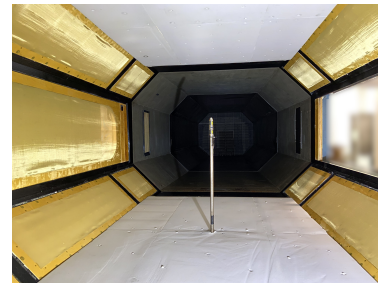$$v(t) = \sum_{f \in F} \sin\left(2\pi f t + \phi_{\text{rand}}\right), \tag{1}$$

2
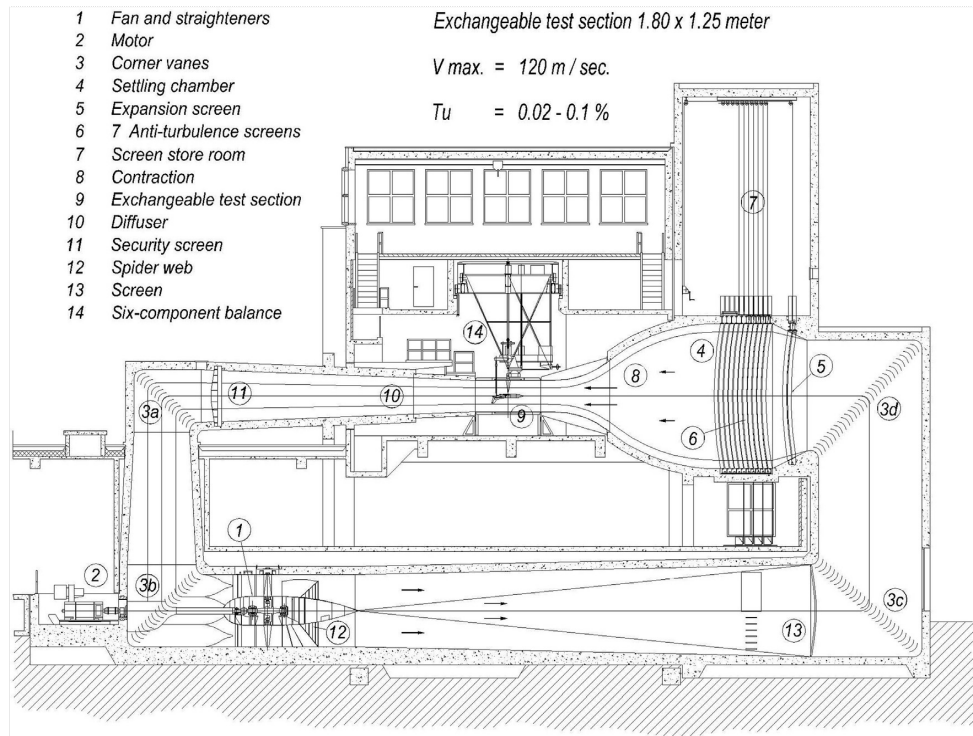
(a) Wind tunnel circuit
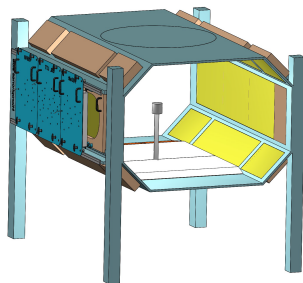
(b) Test section CAD **(c) Without lining** **(d) With lining**

Fig. 1   Low turbulence tunnel circuit (top) [22], and aeroacoustic test section, as seen from the inlet: CAD of the test section (bottom–left), test section with baseline reflective walls (bottom–centre) and fully lined test section (bottom–right).

where $F = \{f_1, f_1 + 5\,\text{Hz}, f_1 + 10\,\text{Hz}, ..., f_{\text{end}}\}$, ϕ_{rand} is a random phase shift applied to each sinusoid, and t is the time coordinate.

2. Aeroacoustic test section lining

The experimental campaign evaluates four different test section configurations (Table 1). The baseline (most reflective configuration) is seen in Fig. 1c. The octagonal baseline test section contains 7 solid fully reflective walls. The Kevlar left side–panel is present in all four configurations, to allow measurements with the microphone array. The plate that holds the microphones is lined with 5 cm thick plane Basotect melamine. The most anechoic configuration (Figs. 1b and 1d), has the floor and ceiling lined with 3 cm Basotect melamine foam. The lining is extruded from the baseline surfaces. Ramps are designed upstream and downstream of the lining, to prevent strong aerodynamic loads on the lining, and an increase in background noise, e.g. due to separation. On the 5 side walls opposite and adjacent to the array, the baseline panels are substituted with lined panels. These lined side–panels consist of 5 cm thick wedged Basotect melamine, covered with a Kevlar sheet. Two intermediate test sections were also tested: one with the top and

3

bottom flat melamine lining, and with the baseline side–panels, and the second with the baseline top and bottom, and with the lined side–panels.

Table 1   Low Turbulence Tunnel test sections tested

Test section	Microphone array recessed behind Kevlar	Top and bottom flat 3 cm melamine lining	Side–panels lined with 5 cm wedged melamine, covered by Kevlar
A, Baseline	✓	-	-
B, Intermediate	✓	✓	-
C, Intermediate	✓	-	✓
D, most Anechoic	✓	✓	✓

The melamine foam's viscous and inertial resistivities are, respectively, $R_v = 9\,\mathrm{kPa\,s\,m^{-2}}$ and $R_i = 2\,\mathrm{kPa\,s^2\,m^{-3}}$ [17]. The high viscous resistivity of the melamine foam leads to a high acoustic absorption. Figure 2 shows the reflection characteristics of the melamine lining, when placed in front of a solid wall, and considering a 90° reflection. The experimental values were obtained from normal-incidence impedance tube measurements at the Netherlands Aerospace Centre (NLR). The empirical values were obtained from Delany's empirical model for surface impedance, $\underline{Z}_S$ [24]. The complex reflection coefficient, $\underline{R}_c$, was obtained from [24]:

$$\underline{R}_c(f) = \frac{\underline{Z}_s(f) - Z_0}{\underline{Z}_s(f) + Z_0}, \tag{2}$$

where f is frequency and Z_0 is the impedance of air. Figure 2 shows that the thicker melamine lining leads to a higher reflection mitigation, specially at frequencies below 2 kHz.

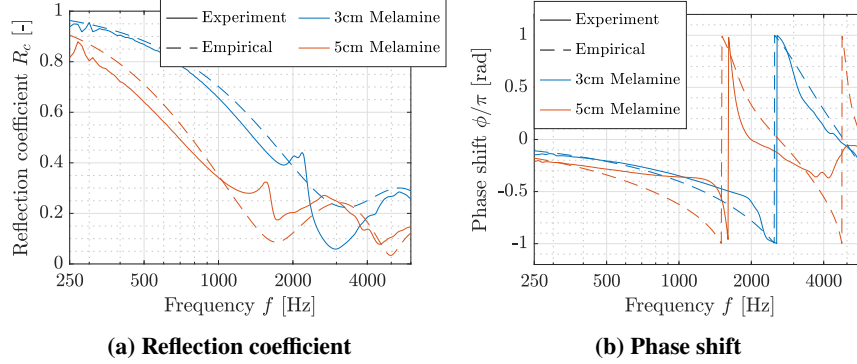**(a) Reflection coefficient** **(b) Phase shift**

Fig. 2   Acoustic characterization of the plane Basotect melamine foam. Absolute reflection coefficient (left) and phase shift at the foam surface (right) for a normal incidence reflection.

B. Acoustic Measurement Technique

The acoustic measurements were taken with a phased microphone array. The array consists of 62 PUI AUDIO 665–POM–2735P–R microphones. The array has an elliptical shape, extending 1.6 m in the streamwise direction and 0.4 m in the vertical direction, and is shown in Fig. 3a. The microphones are held by a solid plate, lined with 5 cm plane melamine foam. The microphones are positioned flush with the foam surface. During measurements, the microphones are recessed 15 cm behind a stretched Aviation-standard Kevlar 49 T 965 sheet (see Figs. 1 and 3b). The microphones were calibrated with a Brüel & Kjaer 4230 pistonphone, at the frequency of 1 kHz. Each measurement was taken with a measurement time of 20 s and a sampling frequency of 50 kHz.
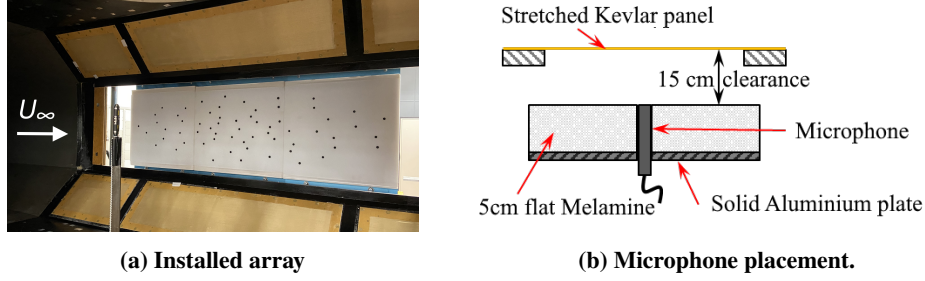
4

(a) Installed array   **(b) Microphone placement.**

Fig. 3   Low Turbulence Tunnel microphone array: array installed in test section C, without the array's Kevlar panel (left); and microphone placement, behind the Kevlar panel (right). Figure b) adapted from [25].

C. Geometric modelling

The primary acoustic reflections in the LTT test section, from the source to the microphone array, were predicted with a geometric modelling (GM) algorithm. The algorithm is an extension of the geometric model described in Ref. [17]. The algorithm is based on the mirror–source method, and therefore considers reflections in the test section to be specular, neglecting the existence of diffuse reflections. Diffraction inside the test section is also neglected in the present geometric model. The mirror-source method assumes the walls of the test section to be infinite, and loses accuracy at lower frequencies, when the acoustic wavelength becomes comparable to the size of the wall [26]. The method provides a good initial prediction of acoustic reflections on a single wall, with similar dimensions to the dimensions of the LTT test section walls (i.e. of the same order of magnitude), for both fully reflective and lined (with melamine foam) cases [17].

The LTT test section has an octagonal shape, as seen in Fig. 1. The primary reflections on the three larger walls of the test section (floor, ceiling and wall opposite to the array) are modelled as a mirror–source, as shown in Fig. 4. The effect of lining was taken into account by considering the complex valued surface reflection coefficient of the lined walls. The experimental reflection coefficients shown in Fig. 2 were used in the algorithm, by adjusting the amplitude and phase of each mirror reflection signal, $\underline{S}_{MR}(f)$, with respect to the direct source signal, $\underline{S}_{DS}(f)$:

$$\underline{S}_{MR}(f) = \underline{S}_{DS}(f)\underline{R}_c(f). \tag{3}$$

By considering the $\underline{R}_c(f)$ of Fig. 2, the lining on the wall opposite to the array was simplified with respect to the experiment, from 5 cm wedged melamine (covered by Kevlar) to 5 cm plain melamine. As in [17], for the flow-on cases, the path and propagation time of each sound ray from the mirror source to the receivers (microphones) is re-calculated taking into account convection by the flow.
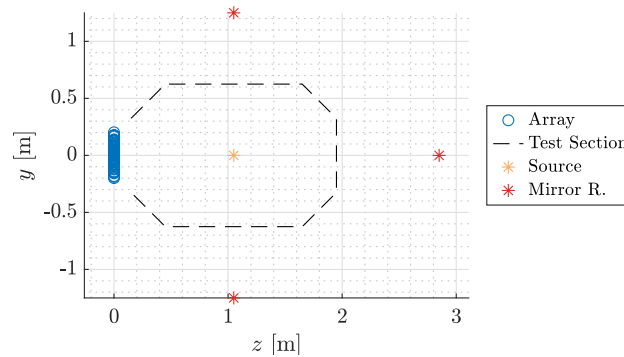

Fig. 4   Setup for the geometric modelling simulations.

D. Signal processing

The data was recorded with the 62 array microphones. The spectra of the isolated microphones were obtained with the Welch's method [27]. The 20 s signals were divided into chunks of 0.1 s, with a 50 % overlap. Each chunk was

5

multiplied by the Hanning window. The spectrograms analysed in the study were obtained by dividing the 20 s signals in time blocks of 0.05 s, with 50 % overlap. Sound Pressure Level, SPL, was defined as:

$$\text{SPL} = 20 \log_{10} \left(\frac{p'_{\text{rms}}}{p_{\text{ref.}}} \right), \tag{4}$$

where p'_{rms} is the root mean square of the pressure fluctuations, and the reference pressure, $p_{\text{ref.}}$, is 2×10^{-5} Pa.

Acoustic interference in the test section was quantified by the difference between the measurements in the reverberant environment and the reference speaker measurement, which was taken outside the wind tunnel test section, in a large room (with low reverberation) and with the microphone array described in Sec. II.B. ΔSPL is defined as:

$$\Delta\text{SPL} = \text{SPL}_{\text{Speaker inside the test section}} - \text{SPL}_{\text{Reference, speaker}}, \tag{5}$$

being positive and negative ΔSPL, respectively, indicative of constructive and destructive interference between direct source and reflections, at the measurement location. ΔSPL $= 0$ indicates that, at that specific frequency, the measurement inside the test section is not disturbed by reflections.

1. Conventional Beamforming

The acoustic data from the microphone array was processed with conventional frequency domain beamforming. Conventional beamforming (CBF) is a robust and fast method for identifying sound sources, and for determining source power levels. CBF is a widely used method in aeroacoustic studies [9]. The signals from the microphone array are processed in the frequency domain:

$$\boldsymbol{p}(f) = \begin{pmatrix} p'_1(f) \\ \vdots \\ p'_N(f) \end{pmatrix}, \tag{6}$$

where p'_n is the pressure fluctuation recorded at each microphone, n. N stands for the number of microphones in the array. The propagation of the sound wave is considered in beamforming in the definition of the steering vector, $g_{j,n}$. The steering vector takes into account the sound wave's spherical spreading and phase shift from a scan grid point, j, to a microphone n. $g_{j,n}$ is the Green's function of the sound propagation from a free-field monopole source:

$$g_{j,n} = \frac{\exp\left(-2\pi i f \Delta t_{j,n}\right)}{\left\| \boldsymbol{x}_n - \xi_j \right\|}, \tag{7}$$

where $\Delta t_{j,n} = \left\| \boldsymbol{x}_n - \boldsymbol{\xi}_j \right\|/c$ is the sound propagation time from the grid point location ξ_j to the receiver at x_n. c is the speed of sound. $\|\cdot\|$ is the Euclidean norm of a vector. For the flow–on cases, $\Delta t_{j,n}$ was recalculated taking into account the flow convection of sound waves. The vector $\boldsymbol{x}_n$ contains the coordinates of all microphones in the array. For each grid point, the noise levels are estimated from:

$$A\left(\boldsymbol{\xi}_j\right) = \frac{\boldsymbol{g}_j^*(\boldsymbol{p}\boldsymbol{p}^*)\boldsymbol{g}_j}{\left\| \boldsymbol{g}_j \right\|^2}, \tag{8}$$

$\boldsymbol{p}\boldsymbol{p}^*$ is a $N \times N$ matrix, commonly referred to as cross-spectral matrix (CSM), where the asterisk, $(\cdot)^*$, represents the complex conjugate transpose.

The beamforming data were processed considering two different scan grids. For identifying the sound sources in the empty test section, a 3D scan grid was designed, which covers the 8 walls of the octagonal test section. This grid can be visualised in Fig. 5. For estimating the noise levels of the speaker, when installed in the test section, a 2D plane parallel to the array was considered (see Fig. 6). The 2D grid is at a 1.05 m distance from the array, and passes through the spanwise centre of the test section, i.e. through the speaker location. After calculating the beamforming maps, the speaker noise levels were obtained with the Source Power Integration (SPI) method [28]. The experimental CSM is normalised with the CSM of a simulated point monopole source, with known noise levels, in order to quantify the noise levels of the experimental source:

$$A_{\text{SPI}}(f) = \frac{\sum_{j=1}^{K} \boldsymbol{g}_j^*(\boldsymbol{p}\,\boldsymbol{p}^*)_{\text{exp.}}\boldsymbol{g}_j}{\sum_{j=1}^{K} \boldsymbol{g}_j^*(\boldsymbol{p}\,\boldsymbol{p}^*)_{\text{sim.}}\boldsymbol{g}_j}, \tag{9}$$

where K is the number of grid points considered in the source power integration. Figure 6 shows the beamforming map of the reference speaker measurement. The 12×12 cm source power integration region is illustrated.
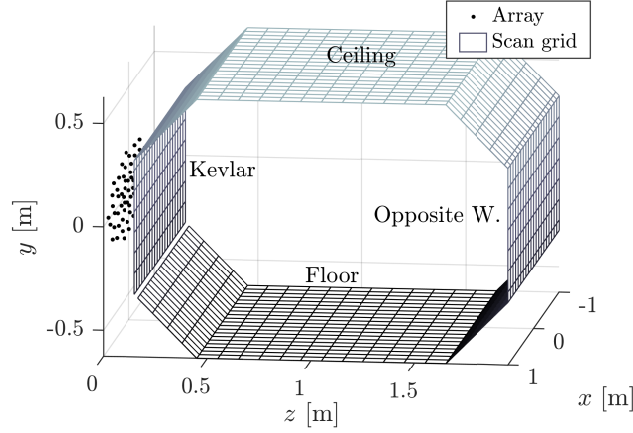

Fig. 5   Scan grid along the 8 walls of the LTT test section. Microphone array located behind the Kevlar panel, which is also evaluated with the grid.
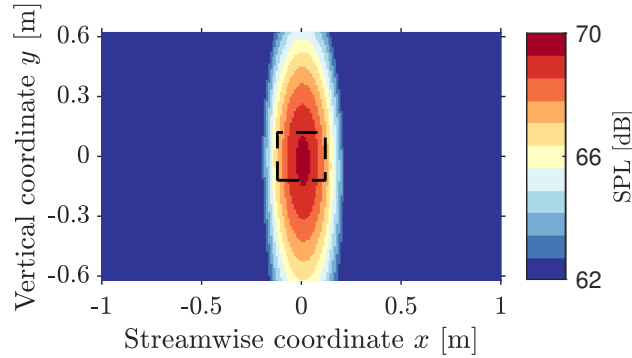

Fig. 6   Beamforming map of the reference speaker measurement, for the 1 kHz centered third–octave band. Speaker located at a 1.05 m distance from the array. The source power integration region is indicated by the dashed line.

III. Wind tunnel acoustic characterization

The present section analyses the results obtained from the experimental data, and compares these with the results obtained from the geometric modelling tool. The acoustic properties of the tunnel are characterized by analysing the acoustic reflections in the test section (Sec. III.A). The background noise is analysed in Sec. III.B by evaluating speaker–off measurements. In Section III.C, the measurements with the flow and speaker –on are analysed.

A. Acoustic reflections in the wind tunnel circuit

The prolongation of sound, due to reflections in the wind tunnel circuit, was analysed with intermittent speaker measurements. During these measurements, the speaker was paused at the time t_0. To characterize the reverberation

7

for the different test section configurations, the spectrogram of the data was produced. The spectrograms of Fig. 7 were obtained by averaging the sound powers obtained from all the microphones in the array, for each timestep, being therefore indicative of the acoustic energy in the test section. The results are shown for the third-octave band centres, $f_{1/3}^{\text{cen.}}$. Test section C, which has the baseline top and bottom, and lining on the side–panels (see Table 1), was also tested outside the wind tunnel circuit (Fig. 7e). The reverberation time, T_{25}, is also shown in Fig. 7. T_{25} is the time in which the overal sound pressure level reduces by 25 dB, after turning off the speaker. T_{25} was calculated considering the frequencies shown in Fig. 7.

Figure 7 shows that both the flat melamine (top and bottom lining) and the lined side–panels are efficient in reducing reverberation in the test section, as reverberation reduces faster in Figs. 7b and 7c than in Fig. 7a. There is however little difference between the performance of the two lining solutions in reducing reverberation, as Figs. 7b and 7c show a similar pattern. When both linings are used simultaneously, the improvement in reducing reverberation is further noticeable (see Fig. 7d). The linings are particularly efficient at reducing reverberation at high frequency, which is consistent with the reflection coefficients shown in Fig. 2. Figure 7e indicates that reverberation in the test section is negligible, when the test section is placed outside the tunnel circuit. The reverberation time, for the test sections installed in the wind tunnel circuit, is considerably longer than at other facilities commonly used for aeroacoustics research, e.g. TU Delft's Anechoic Tunnel ($T_{60,\text{A-Tunnel}} = 0.22$ s) [29]. The results suggest that it can be advantageous to line further sections of the tunnel circuit, e.g. the diffuser (see Fig. 1a).

(a) Baseline test section

(b) Flat melamine lining (top and bottom)

(c) Kevlar side–panels

(d) Most anechoic test section

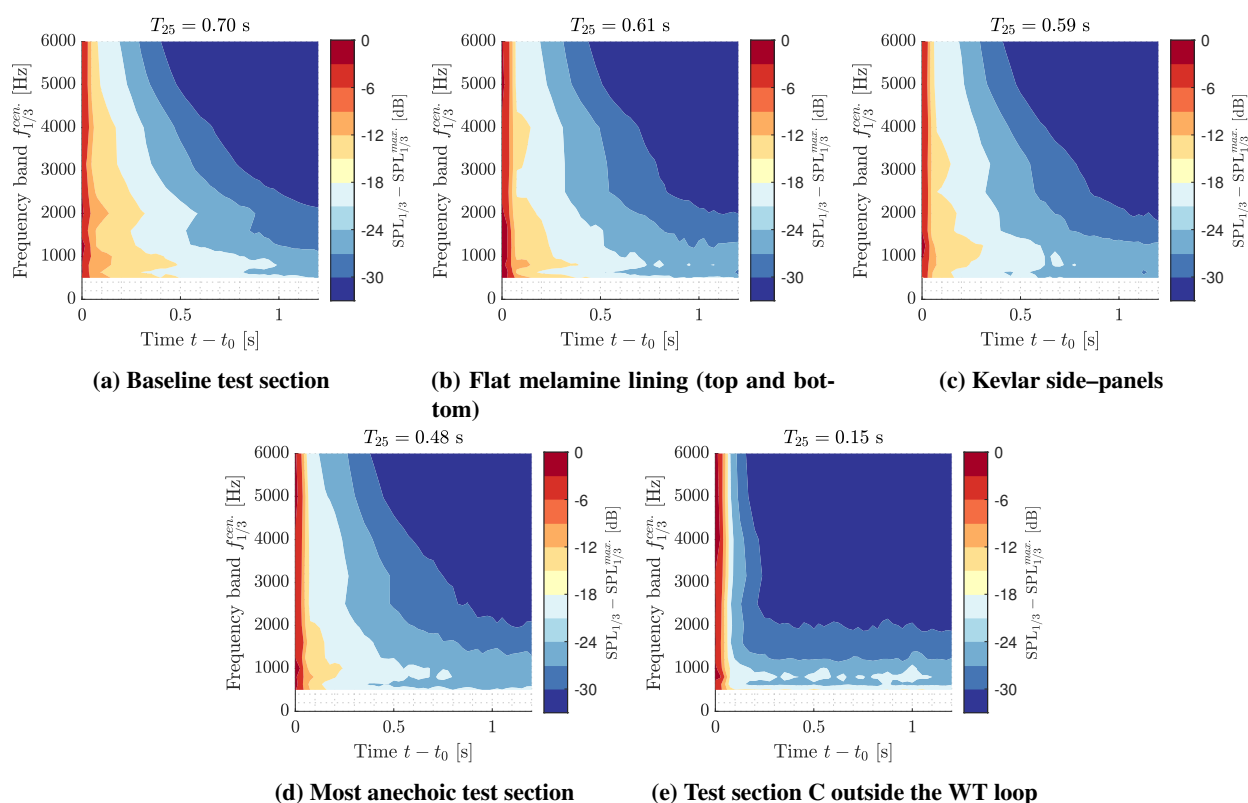**(e) Test section C outside the WT loop**

Fig. 7 Spectrogram of the acoustic data obtained from the intermittent speaker tests. The spectrogram shows the development of reverberation in the test section from the moment the speaker is interrupted. The plots a) to d) refer to the test cases with the LTT test section installed in the tunnel circuit: test sections A (top–left), B (top–centre), C (top–right), D (bottom–left). Test section C, with the wedged melamine Kevlar side–panels, was also tested outside the wind tunnel circuit (bottom–right).

1. Acoustic interference inside the test section

The present section investigates the acoustic interference that occurs at the microphone array location, between a direct sound source and reflections in the circuit. The objective is to quantify the disturbance caused by primary

reflections, which directly reflect towards the microphones, by secondary reflections (here meant as any non-primary reflections) in the test section, and by reverberation caused by the remaining parts of the circuit. The final goal is to identify which parts of a closed tunnel are beneficial to treat with acoustically absorbent materials.

Reflections inside the test section lead to frequency dependent constructive or destructive interference patterns at the microphone locations. Figure 8 shows the interference mitigation achieved with lining, from both experimental and simulation data. The spectra were obtained by averaging the source powers between all microphones in the array. A good test section acoustic performance is reached when ΔSPL becomes close to 0 dB.

(a) GM simulation of primary reflections   **(b) Experiment: installed vs. uninstalled**

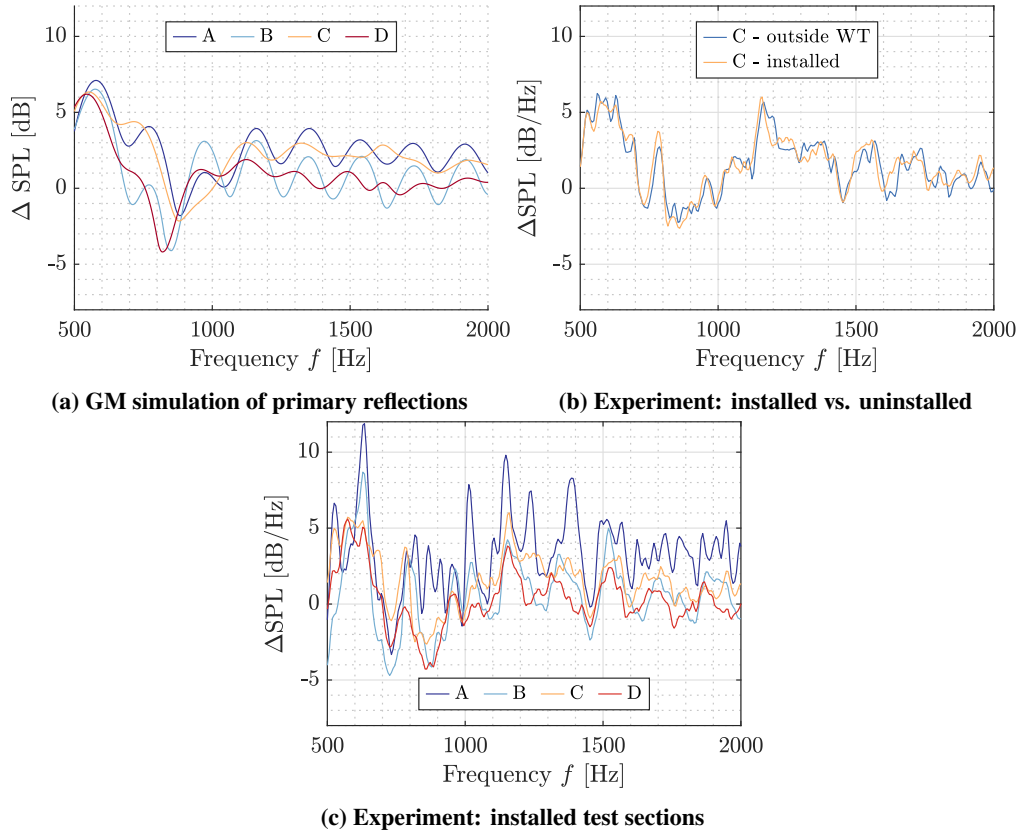**(c) Experiment: installed test sections**

Fig. 8   Acoustic interference caused by the reflections: difference between the measurement inside the test section and the reference speaker measurement. Primary reflections in the test section, simulated with geometric modelling (top–left); difference between installed and uninstalled test section, from experimental data (top–right); and each installed test section, from experimental data (bottom). Average from the 62 microphones in the array.

Figure 8a shows the acoustic interference caused by the three primary (specular) reflections in the test section that reach the microphone array from the acoustic source (see the GM setup in Fig. 4). The figure shows that, for the four test sections, the primary reflections cause a strong constructive interference peak for frequencies in the vicinity of 600 Hz, which is followed by a destructive interference peak, near 800 Hz. Below 1000 Hz, the reflection coefficient of the lined walls is still relatively high (see Fig. 2). Above 1000 Hz, Fig. 8a shows that, for the baseline test section (A), the interference caused by the primary reflections is approximately 3 dB. For the most anechoic configuration, configuration D, ΔSPL becomes close to 0 dB at high frequencies. The result of Fig. 8a shows that reducing the reflection coefficient of the test section walls which cause the primary reflections is crucial for achieving accurate acoustic measurements.

Figure 8b shows the acoustic interference patterns which occur in test section C, for the case where the test section is installed in the tunnel circuit, and for the case where the test section is outside the circuit. As seen from Fig. 7, the wind tunnel circuit is responsible for a long reverberation time, when the test section is installed. However, Fig. 8b indicates that installing the test section in the wind tunnel circuit does not change the dominant acoustic interference phenomena. The result indicates that, at these frequencies, and in the absence of aerodynamic background noise in the tunnel, reverberation caused by the remaining parts of the circuit (besides the test section) is not visible in the acoustic

9

measurements.

Figure 8c, obtained from the experimental measurements with the test sections installed, presents the acoustic interference pattern caused by primary and secondary reflections in the test section, and by reverberation in the tunnel. The comparison of Figs. 8a and 8c shows that the experimental ΔSPL is noisier than for the simulated case, where only the primary reflections are present. This is associated with the fact that, besides likely experiencing diffraction, reflections in the experimental case are infinite. The experimental ΔSPL is also higher: for the baseline configuration, the difference with respect to the reference measurement is, for a wide range of frequencies, close to 5 dB. For the lined cases, the experimental ΔSPL is non-negligible also at high frequencies, when the primary reflections on the lined walls are relatively weak. This result indicates that secondary reflections in the test section (i.e. any non-primary reflections) noticeably affect the transfer function from the source to the microphone array. Figure 8 shows that it is beneficial to line as much area of the test section walls as possible, for reducing acoustic interference at the measurement location.

B. Aerodynamic noise sources

Figure 9 shows the beamforming maps of the empty test section measurements, with the wind tunnel operating at $U_\infty = 40\,\text{m s}^{-1}$. The scan plane is placed along the test section walls (see Fig. 5). For the four test sections, the beamforming maps indicate that most background noise originates from downstream of the test section (where $x < -1\,\text{m}$). This can be e.g. from the diffuser's boundary layer, or discontinuities in the circuit, such as a gap between the test section and the diffuser. Furthermore, the result indicates noise sources at the Kevlar panel location. The figure also shows that, when lined, the noise from a given wall/ side–panel is reduced. This occurs despite of the higher surface roughness of the liner with respect to a solid wall, which increases boundary layer turbulence [17]. Figures 9c and 9d show the strong reduction in noise from the opposite wall, when the lined side panels are installed. This can be explained by the reduction in reflection of background noise at the opposite wall, when the wall's reflection coefficient is reduced.
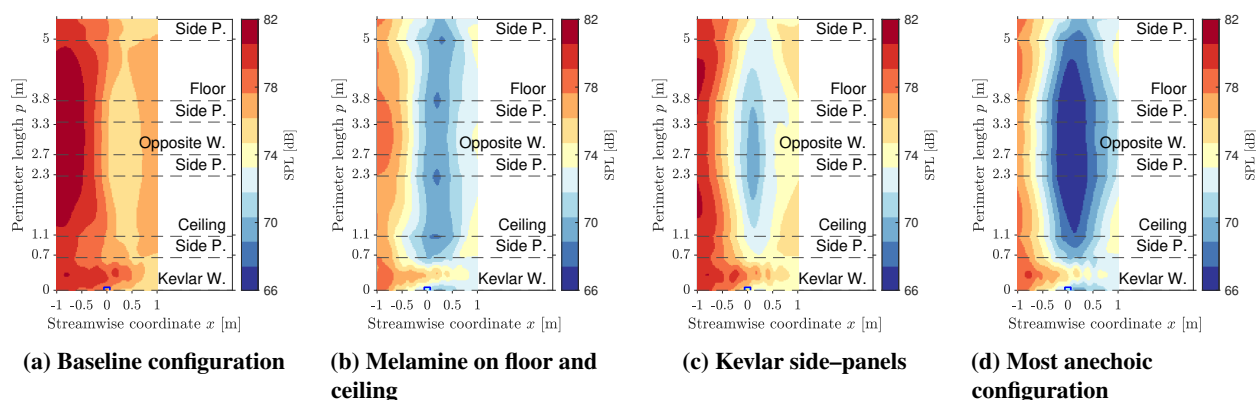

(a) Baseline configuration

(b) Melamine on floor and ceiling

(c) Kevlar side–panels

(d) Most anechoic configuration

Fig. 9   Beamforming along the (empty) test section walls, for the 1 kHz third–octave band. Free-stream velocity 40 m s^{-1}. Test sections A (left), B (centre–left), C (centre–right) and D (right).

Figure 10 shows the background noise of the empty test sections, at $U_\infty = 20\,\text{m s}^{-1}$ and $U_\infty = 40\,\text{m s}^{-1}$. Test sections A and C operated with the wind tunnel fan at a higher angular velocity than B and D, for reaching the same U_∞. Test sections B and D include the top and bottom flat melamine panels, which reduce the effective cross–sectional area of the tunnel, without noticeably increasing the pressure loss in the circuit. For test sections B and D, a lower wind tunnel fan rotational speed, Ω, is therefore required. As a consequence of the higher wind tunnel fan power setting, test sections A and C feature the highest background noise. This result indicates that the aerodynamic background noise sources produced in the wind tunnel circuit, outside the test section, are dominant at the array location. These noise sources can be e.g. the wind tunnel fan, or physical discontinuities throughout the circuit. The scaling, k, of the aerodynamic noise levels with free-stream velocity was obtained from:

$$\left(\frac{U_{\infty,2}}{U_{\infty,1}}\right)^k = \left(\frac{p'_{\text{rms},2}}{p'_{\text{rms},1}}\right)^2, \tag{10}$$

where p'_{rms} was calculated considering the frequencies shown in Fig. 10. The high SPL peaks at $f = 600\,\text{Hz}$, for the measurements at $U_\infty = 20\,\text{m s}^{-1}$, have been previously identified to originate from electrical devices used to power

10

the wind tunnel [30]. The third octave frequency band centered at $f = 630\,\text{Hz}$ has therefore been filtered out, for the calculation of k. For the four test sections, k has a value between 4 and 5. This indicates that most aerodynamic noise is generated due to fluid–solid interaction. A value of $k = 8$ is considered to be ideal for aeroacoustic wind tunnels, since it is indicative that jet–noise has the strongest contribution to aerodynamic noise [29].

Figure 10 also shows that installing the wedged melamine Kevlar side–panels (compare e.g. test sections A and C) reduces the background noise by approximately $1 - 2\text{dB}$. This result is consistent with the lower levels found in the beamforming maps of Fig. 9, for the test sections with lined side–panels. The results of Figs. 9 and 10 highlight the effectiveness of test section lining solutions, for reducing the disturbance caused by background noise on acoustic measurements.
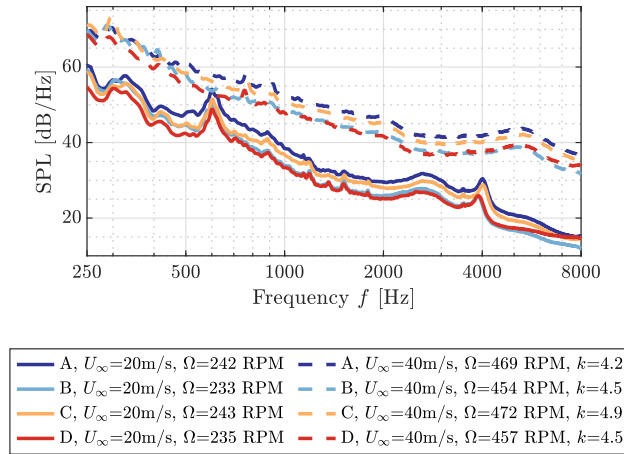

Fig. 10 **Background noise of the 4 empty test sections, at $U_\infty = 20\,\text{m s}^{-1}$ and $U_\infty = 40\,\text{m s}^{-1}$. Average between the 62 microphones in the array. The angular velocity of the wind tunnel fan, for each test, is specified in rotations per minute (RPM).**

C. Acoustic wind tunnel measurements - with flow

The effect of having the wind tunnel flow–on on the acoustic measurement of a source inside the test section was initially assessed with geometric modelling. The simulated spectra of Fig. 11 were obtained from source power integration of the beamforming maps of simulated data. The results obtained for the baseline (Fig. 11a) and most anechoic (Fig. 11b) test sections show that, up to $U_\infty = 30\,\text{m s}^{-1}$, i.e. at relatively low wind tunnel free-stream Mach number ($M = U_\infty/c = 0.09$), the convection of the sound waves by the flow does not affect the acoustic interference pattern at the microphone array location. At higher Mach number ($M = 0.29$), the convection caused by the flow causes a significant shift of the interference pattern. The intensity of the mirror sources, as perceived by the microphones, is however not visibly affected, as the magnitude of the interference peaks remains unchanged.

Figure 12 shows the SPI spectra obtained experimentally with each test section configuration, for the free-stream velocities: $U_\infty = 0\,\text{m s}^{-1}$, $U_\infty = 20\,\text{m s}^{-1}$ and $U_\infty = 30\,\text{m s}^{-1}$. Below $1\,\text{kHz}$, the broadband and the white noise signals emitted by the speaker are relatively low, in comparison with the background noise. Therefore, the experimental spectra of Fig. 12 in the ranges $500\,\text{Hz}$ to $800\,\text{Hz}$, $800\,\text{Hz}$ to $1000\,\text{Hz}$, and $1000\,\text{Hz}$ to $2000\,\text{Hz}$ correspond, respectively, to the measurements with the speaker emitting the low–frequency narrow band noise, the mid–frequency narrow band noise, and broadband noise (see description of the signals in Sec. II.A.1).

In agreement with the geometric modelling data, the experimental data indicates that the magnitude and the frequencies of the acoustic interference peaks remain unchanged, at low free-stream velocities. The spectra of Fig. 12 also show that, at $U_\infty = 30\,\text{m s}^{-1}$, there are frequencies for which the SPL is higher for the flow–on case than at $U_\infty = 0\,\text{m s}^{-1}$ (most noticeable for f close to $850\,\text{Hz}$). This indicates that, at these frequencies, the background noise is comparable or higher than the noise levels from the acoustic source. The disturbance caused by the aerodynamic background noise in the measurement is most noticeable for the baseline test section configuration (Fig. 12a), which is consistent with the higher background noise levels seen in Figs. 9 and 10, for this test section.

The results of Figs. 11 and 12 show that, for aeroacoustics experiments at relatively low free-stream velocity ($M < 0.1$), the disturbance on acoustic measurements caused by reflections in the test section can be assessed without

11

flow. The limit for which the flow–off acoustic measurements are valid can be investigated with a geometric modelling algorithm, based on the mirror–source method.

(a) Baseline test section - A
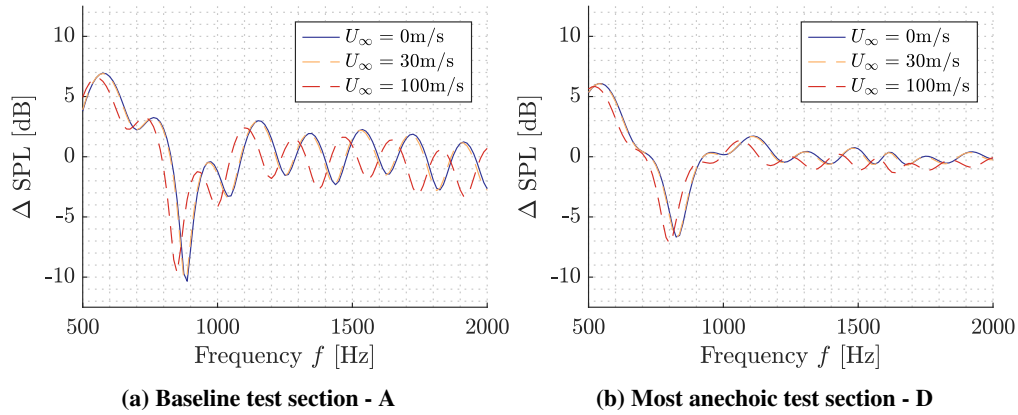
(b) Most anechoic test section - D

Fig. 11   Acoustic interference caused by the primary reflections, in the geometric modelling data, for varying free-stream velocity in the test section. Baseline test section (left), and most anechoic test section configuration (right). Spectra obtained from source power integration of the beamforming maps.
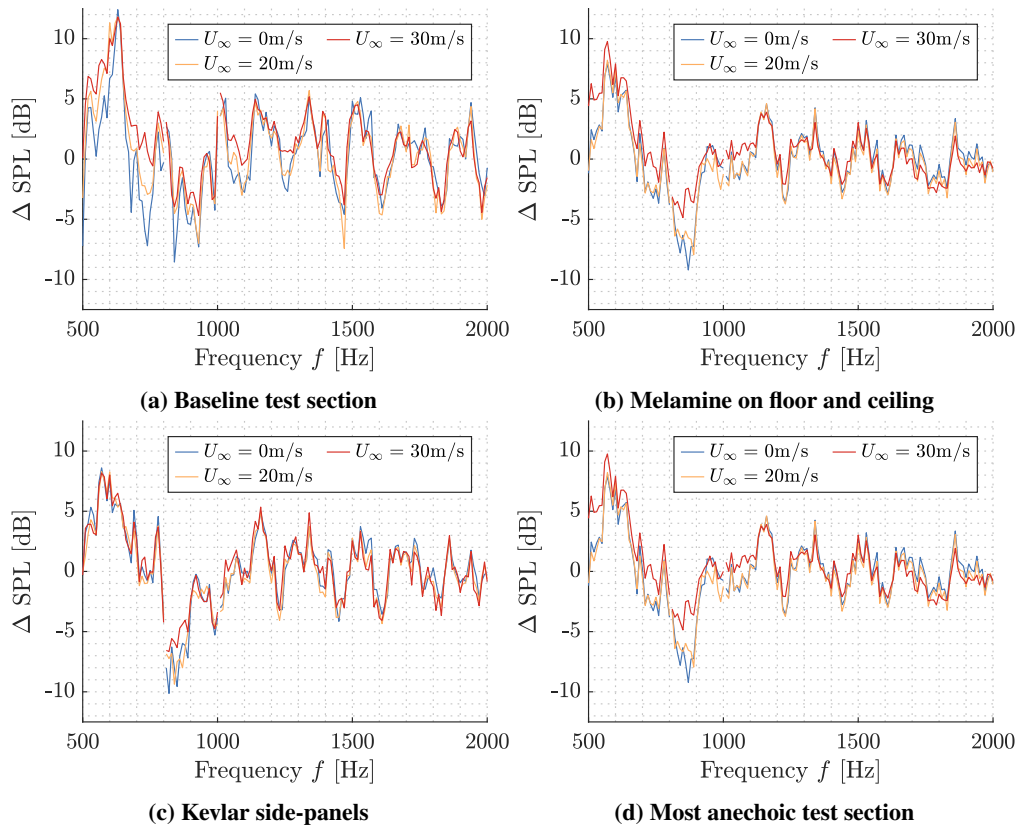

(a) Baseline test section

(b) Melamine on floor and ceiling

(c) Kevlar side-panels

(d) Most anechoic test section

Fig. 12   Acoustic interference caused by the reflections, in the experimental data. Test sections A (top–left), B (top–right), C (bottom–left) and D (bottom–right). Spectra obtained from source power integration of the beamforming maps.

12

IV. Conclusion

An experimental campaign was conducted in TU Delft's closed test section Low Turbulence Tunnel. Four test section configurations were tested, as the test section was progressively lined with sound absorbing treatments. An omnidirectional speaker was used as reference acoustic source. The resulting acoustic signals were measured with a phased microphone array. The disturbance in the acoustic measurement of the source signal was analysed by assessing the effect of reflections in the test section, reverberation in the wind tunnel, convection of acoustic waves by the free-stream flow, and aerodynamic background noise. A geometric modelling algorithm was developed for predicting the disturbance caused by primary reflections in the test section on acoustic measurements, for each lining configuration.

The experimental results show that reverberation in the wind tunnel circuit is reduced with test section lining. Reverberation caused by walls outside the test section (both upstream and downstream), although strong, is shown to cause a negligible disturbance in the microphone array measurements, in the flow–off tests. For the flow–on experimental measurements, aerodynamic noise originating outside the test section was identified to be a dominant cause of pressure fluctuations at the array location. Lining over the test section walls was an effective approach for reducing the aerodynamic noise reaching the microphones. The geometric modelling results demonstrate that a strong improvement of the acoustic capabilities of a wind tunnel can be achieved, by reducing the reflection coefficient of the test section walls for which there is a direct reflection path from the source to the microphone array. The experimental acoustic tests show that the remaining test section walls should also be lined, for approaching anechoic conditions in the test section. The convection of sound waves by the free-stream flow, at low Mach number ($M < 0.1$), was demonstrated to cause a negligible change in the acoustic interference pattern at the microphone array.

Based on the results of this study, it can be concluded that acoustic reflections in a wind tunnel designed for aeroacoustic studies can be investigated with a speaker, without flow. The flow conditions for which the flow–off acoustic measurements are valid should be assessed, e.g. with a geometric modelling algorithm. Measurements of aerodynamic background noise should be performed with an empty test section, and lining can be used to reduce the background noise that reaches the microphone array. Future studies should investigate the benefits obtained from lining other sections of the tunnel, such as the diffuser, for reducing aerodynamic noise in the circuit. The use of higher fidelity methods for predicting acoustic interference in the test section is also expected to further help with designing acoustically treated test sections.

Acknowledgments

References

[1] Merino-Martinez, R., van der Velden, W., Avallone, F., and Ragni, D., "Acoustic measurements of a DU96-W-180 airfoil with flow-misaligned serrations at a high Reynolds number in a closed-section wind tunnel," *7th International Conference on Wind Turbine Noise Rotterdam*, 2017.

[2] Rubio Carpio, A., Merino Martínez, R., Avallone, F., Ragni, D., Snellen, M., and van der Zwaag, S., "Experimental characterization of the turbulent boundary layer over a porous trailing edge for noise abatement," *Journal of Sound and Vibration*, Vol. 443, 2019, pp. 537–558. doi:10.1016/j.jsv.2018.12.010, URL https://doi.org/10.1016/j.jsv.2018.12.010.

[3] Oerlemans, S., Broersma, L., and Sijtsma, P., "Quantification of Airframe Noise Using Microphone Arrays in Open and Closed wind Tunnels," *International Journal of Aeroacoustics*, Vol. 6, No. 4, 2007, pp. 309–333. doi:10.1260/147547207783359440.

[4] Sinnige, T., Ragni, D., Malgoezar, A. M. N., Eitelberg, G., and Veldhuis, L. L. M., "APIAN-INF: an aerodynamic and aeroacoustic investigation of pylon-interaction effects for pusher propellers," *CEAS Aeronautical Journal*, Vol. 9, No. 2, 2018, pp. 291–306. doi:10.1007/s13272-017-0247-2.

[5] Cattafesta, L., Bahr, C., and Mathew, J., "Fundamentals of Wind-Tunnel Design," *Encyclopedia of Aerospace Engineering*, 2010. doi:10.1002/9780470686652.eae532.

[6] Devenport, W. J., Burdisso, R. A., Borgoltz, A., Ravetta, P. A., Barone, M. F., Brown, K. A., and Morton, M. A., "The Kevlar-walled anechoic wind tunnel," *Journal of Sound and Vibration*, Vol. 332, No. 17, 2013, pp. 3971–3991. doi: 10.1016/j.jsv.2013.02.043, URL http://dx.doi.org/10.1016/j.jsv.2013.02.043.

[7] Blacodon, D., and Bulté, J., "Reverberation cancellation in a closed test section of a wind tunnel using a multi-microphone cesptral method," *Journal of Sound and Vibration*, Vol. 333, No. 9, 2014, pp. 2669–2687. doi:10.1016/j.jsv.2013.12.012, URL http://dx.doi.org/10.1016/j.jsv.2013.12.012.

[8] Soderman, P. T., Schmitz, F. H., Allen, C. S., Jaeger, S. M., Sacco, J. N., and Hayes, J. A., "Design of a deep acoustic lining for the 40- by 80- Foot Wind Tunnel test section," *5th AIAA/CEAS Aeroacoustics Conference and Exhibit*, 1999, pp. 899–918. doi:10.2514/6.1999-1938.

[9] Merino-Martínez, R., Sijtsma, P., Snellen, M., Ahlefeldt, T., Antoni, J., Bahr, C. J., Blacodon, D., Ernst, D., Finez, A., Funke, S., Geyer, T. F., Haxter, S., Herold, G., Huang, X., Humphreys, W. M., Leclère, Q., Malgoezar, A., Michel, U., Padois, T., Pereira, A., Picard, C., Sarradj, E., Siller, H., Simons, D. G., and Spehr, C., "A review of acoustic imaging methods using phased microphone arrays (part of the "Aircraft Noise Generation and Assessment" Special Issue)," *CEAS Aeronautical Journal*, Vol. 10, No. 1, 2019, pp. 197–230. doi:10.1007/s13272-019-00383-4, URL http://dx.doi.org/10.1007/s13272-019-00383-4.

[10] VanDercreek, C. P., Merino-Martínez, R., Sijtsma, P., and Snellen, M., "Evaluation of the effect of microphone cavity geometries on acoustic imaging in wind tunnels," *Applied Acoustics*, Vol. 181, 2021. doi:10.1016/j.apacoust.2021.108154.

[11] Mourão Bento, H. F., Vandercreek, C. P., Avallone, F., Ragni, D., and Snellen, M., "Lattice Boltzmann very large eddy simulations of a turbulent flow over covered and uncovered cavities," *Physics of Fluids*, Vol. 34, No. 10, 2022. doi:10.1063/5.0100001.

[12] Luesutthiviboon, S., Malgoezar, A. M., Merino-Martinez, R., Snellen, M., Sijtsma, P., and Simons, D. G., "Enhanced HR-CLEAN-SC for resolving multiple closely spaced sound sources," *International Journal of Aeroacoustics*, Vol. 18, No. 4-5, 2019, pp. 392–413. doi:10.1177/1475472X19852938.

[13] Gomes, J. P., Bergmann, A., and Holthusen, H., "Aeroacoustic wind tunnel design," *CEAS Aeronautical Journal*, Vol. 10, No. 1, 2019, pp. 231–249. doi:10.1007/s13272-019-00372-7, URL http://dx.doi.org/10.1007/s13272-019-00372-7.

[14] Howe, M. S., "Surface pressures and sound produced by turbulent flow over smooth and rough walls," *Journal of the Acoustical Society of America*, Vol. 90, No. 2, 1991, pp. 1041–1047. doi:10.1121/1.402292.

[15] Manes, C., Poggi, D., and Ridolfi, L., "Turbulent boundary layers over permeable walls: Scaling and near-wall structure," *Journal of Fluid Mechanics*, Vol. 687, 2011, pp. 141–170. doi:10.1017/jfm.2011.329.

[16] Suga, K., Matsumura, Y., Ashitaka, Y., Tominaga, S., and Kaneda, M., "Effects of wall permeability on turbulence," *International Journal of Heat and Fluid Flow*, Vol. 31, No. 6, 2010, pp. 974–984. doi:10.1016/j.ijheatfluidflow.2010.02.023, URL http://dx.doi.org/10.1016/j.ijheatfluidflow.2010.02.023.

[17] Bento, H. F., Ragni, D., Avallone, F., Simons, D., and Snellen, M., "Acoustic wall treatments for wind tunnel aeroacoustic measurements," *Applied Acoustics*, Vol. 199, 2022, p. 108989. doi:10.1016/j.apacoust.2022.108989, URL https://doi.org/10.1016/j.apacoust.2022.108989.

[18] de Vries, R., van Arnhem, N., Sinnige, T., Vos, R., and Veldhuis, L. L. M., "Aerodynamic interaction between propellers of a distributed-propulsion system in forward flight," *Aerospace Science and Technology*, Vol. 118, 2021. doi:10.1016/j.ast.2021.107009.

[19] Lima Pereira, L. T., Avallone, F., Ragni, D., and Scarano, F., "A physics-based description and modelling of the wall-pressure fluctuations on a serrated trailing edge," *Journal of Fluid Mechanics*, Vol. 938, 2022, p. A28. doi:10.1017/jfm.2022.173.

[20] Luesutthiviboon, S., Pereira, L. T. L., Ragni, D., Avallone, F., and Snellen, M., "Aeroacoustic Benchmarking of Trailing-Edge Noise from NACA 633 –018 Airfoil with Trailing-Edge Serrations," *AIAA Journal*, Vol. 61, No. 1, 2023, pp. 329–354. doi:10.2514/1.J061630.

[21] Serpieri, J., "Cross-Flow Instability: Flow diagnostics and control of swept wing boundary layers," Ph.D. thesis, Delft University of Technology, 2018. doi:doi.org/10.4233/uuid:3dac1e78-fcc3-437f-9579-048b74439f55.

[22] Llorente, E., and Ragni, D., "Trailing-edge serrations effect on the performance of a wind turbine," *Renewable Energy*, Vol. 147, 2020, pp. 437–446. doi:10.1016/j.renene.2019.08.128, URL https://doi.org/10.1016/j.renene.2019.08.128.

[23] QSources, "QINDW MINIATURE SOUND SOURCE," , 2022. URL https://www.qsources.be/qindw/.

[24] Aretz, M., Dietrich, P., and Vorländer, M., "Application of the mirror source method for low frequency sound prediction in rectangular rooms," *Acta Acustica united with Acustica*, Vol. 100, No. 2, 2014, pp. 306–319. doi:10.3813/AAA.918710.

[25] Luesutthiviboon, S., and Ragni, D., "Characterization of the Acoustically Treated Low-turbulence Tunnel (LTT) of TU Delft," Hybrid Anechoic Wind Tunnel (HAWT) workshop in 26th AIAA/CEAS Aeroacoustics Conference, Online, 2020.

[26] Savioja, L., and Svensson, U. P., "Overview of geometrical room acoustic modeling techniques," *The Journal of the Acoustical Society of America*, Vol. 138, No. 2, 2015, pp. 708–730. doi:10.1121/1.4926438, URL http://dx.doi.org/10.1121/1.4926438.

[27] Welch, P. D., "The Use of Fast Fourier Transform for the Estimation of Power Spectra: A Method Based on Time Averaging Over Short, Modified Periodograms," *IEEE Transactions on Audio and Electroacoustics*, Vol. 15, No. 2, 1967, pp. 70–73. doi:10.1109/TAU.1967.1161901.

[28] Sijtsma, P., "Phased Array Beamforming Applied to Wind Tunnel and Fly-Over Tests," Tech. Rep. NLR-TP-2010-549, National Aerospace Laboratory (NLR), Amsterdam, The Netherlands, 2010. doi:10.4271/2010-36-0514.

[29] Merino-Martínez, R., Rubio Carpio, A., Lima Pereira, L. T., van Herk, S., Avallone, F., Ragni, D., and Kotsonis, M., "Aeroacoustic design and characterization of the 3D-printed, open-jet, anechoic wind tunnel of Delft University of Technology," *Applied Acoustics*, Vol. 170, 2020. doi:10.1016/j.apacoust.2020.107504.

[30] Luesutthiviboon, S., "Assessing and improving trailing-edge noise reduction technologies for industrial wind-turbine applications," Ph.D. thesis, Delft University of Technology, 2022. doi:10.4233/uuid:23e2f72e-2502-4f4a-9504-ba607bae0364.